AN OPTIMAL REACTIVE POWER CONTROL FOR ISOLATED MODULAR DC/DC CONVERTER SYSTEM

Yi Zhang, Binbin Li, Shaolei Shi, Dianguo Xu

Harbin Institute of Technology, China
Email:zysean@163.com

Abstract

This paper presents an optimal reactive power control in isolated modular DC/DC converter (IMDCC) system based on theoretical and simulated discussions. The system configuration ties two DC grids by using two modular multilevel converters (MMCs) via an AC transformer, which causes the reactive power consuming and will affect the transferrable active power. Then the discussions conclude that the maximum transferrable active power in IMDCC system can be achieved when the reactive power is equally distributed between both MMC stations, which have been ignored by previous research. Finally, the circuit configuration and the control method are described along with simulated and experimental results that verify the effectiveness.

1 Introduction

In recent years, numerous large offshore wind turbines have been built, due to its advantages of higher wind speed, less turbulence, and large areas availability, but most offshore wind farms today are less than 30km from shore using the ac cable collection as well as transmission[1]. The large charging current caused by AC cables imposes restrictions on the transmission voltage level and distance, which is not available for the new trends of long distance and higher power transmission in future large-scale offshore wind farms.

HVDC is a more economical and preferred option for long distance power transmission, but there is a short of DC transformer to connect multi-terminal DC (MTDC) transmission and develop a DC power network[2-4]. In MTDC applications, DC transformers are needed to match the various voltages and exchange power between two dc grids. In addition, DC transformers are also necessary when integrating low-voltage DC sources into HVDC lines or DC loads extracting power from HVDC lines. As for these reasons, presently most of the HVDC installations operate as point-to-point systems, although there has been great incentive for the development of MTDC due to its higher reliability and flexibility.

Over the past few years, many DC transformer topologies
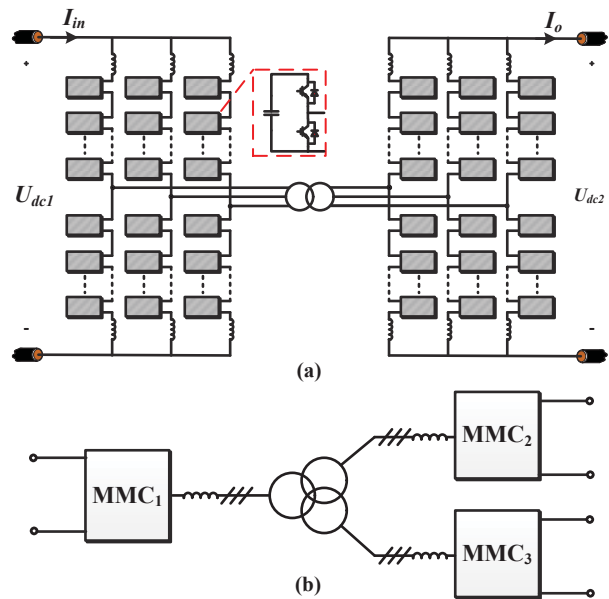
Figure 1: Circuit configuration of the isolated modular DC/DC converter (IMDCC). (a) point-to-point configuration; (b) multi-terminal configuration.

have been introduced, such as resonant DC-DC converter[5], tuned filter modular multilevel DC converter[6], HVDC-DC auto transformer[7,8], input-serial-output-serial dual active bridge[9], etc.. Among them, IMDCC[10] is the most promising topology with both inherent DC faults protection and the flexibility of multi-terminal configuration. Figure 1(a) shows that IMDCC consists of two MMC stations coupled through a galvanic isolation transformer in what might be described as "front-to-front" connection. The transformer provides galvanic separation between the two DC connections as well as the voltage step, where galvanic isolation can be useful in some dc-short condition and for separating grounding arrangements in different parts of a dc network. Additionally, the topology can be utilized as a multi-terminal configuration to connect three or more HVDC lines, see Figure 1(b).

For now, research for IMDCC mainly focus on basic operation[10], carrier frequency optimization[11], and modulations[12]. Until recently, all of these studies have been assumed that the reactive power consuming in the internal of IMDCC is zero, but the reactive power, resulted by both inherent leakage inductance of AC transformer and added inductances in AC sides has an impact on transferrable active power, especially when the AC frequency is higher than 50Hz
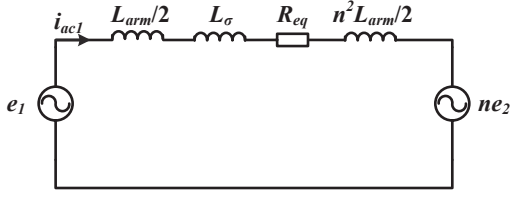
Figure 2: Simplified circuits of the IMDCC referred to the primary side.

or 60Hz (higher AC frequency is beneficial to reduce the volume of the converter). Thus the impact of reactive power should not be ignored from the perspective of practical application. In this paper, we aim to study the influence of the reactive power distribution on the active power transferring capability, in order to figure out the optimal distribution ratio and get the maximum active power transferring capability.

This paper is organized as follows. Section 2 presents the mathematics model of IMDCC system and its theoretical analysis of optimal reactive power distributed ratio. Section 3 explains the control method. The verification of simulation and experiments will be described in section 4. Section 5 summarizes the main findings of this paper.

2 Mathematics model of IMDCC and analysis of optimal reactive power distribution

2.1 Mathematics model of IMDCC

Assuming the AC-side voltages resemble sinusoidal waveforms, the basic operation of one end of IMDCC is similar to the traditional MMC. Taking one phase in both sides of IMDCC for example (see Figure 1), the upper and lower arm voltages u_{uj} and u_{wj} (j=1, 2, where j means primary side and secondary side of IMDCC respectively) are composed of the same dc component $U_{dcj}/2$ and an inverse ac component u_{acj}, which is,

$$\begin{cases} u_{uj} = -u_{acj} + \dfrac{U_{dcj}}{2} \\ u_{wj} = u_{acj} + \dfrac{U_{dcj}}{2} \end{cases} \quad (j=1,2) \quad (1)$$

since the maximum value of u_{uj} and u_{wj} will not exceed $U_{dc1}/2$ or $U_{dc1}/2$, then according to (1), the amplitude of u_{acj} must be less than or equal to $U_{dc1}/2$ or $U_{dc1}/2$.

Similar to the traditional MMC, the arm currents consist of two independent variables, i.e., the output AC current and the circulating current, where the AC current i_{acj} will be distributed evenly in the corresponding upper and lower arms. In addition, each arm current i_{uj} and i_{wj} contains a circulating component i_{cj}. That is,

$$\begin{cases} i_{uj} = \dfrac{i_{acj}}{2} + i_{cj} \\ i_{wj} = -\dfrac{i_{acj}}{2} + i_{cj} \end{cases} \quad (j=1,2) \quad (2)$$

2.2 Simplified equivalent circuit

In IMDCC system described above, its circuit can be simplified as shown in Figure 2, where the transformer can be simplified as a leakage inductor L_σ and the primary-to-secondary winding turns ratio n. Further, L_{arm} is the arm inductor in both sides. Therefore, the total equivalent interconnection inductor L_{eq} referred to the primary side and can be expressed as

$$L_{tot} = \frac{1}{2}L_p + \frac{n^2}{2}L_s + L_\sigma \quad (3)$$

From the simplified equivalent circuit, it can be concluded that the power conversion of an IMDCC system can be viewed as the power exchange between two equivalent AC voltage source e_1 and e_2 through L_{eq}. Thus, the characteristics of the transferred power are determined by e_1 and e_2:

$$L_{eq}\frac{di_{ac1}(t)}{dt} + R_{eq}i_{ac1}(t) = e_1(t) - ne_2(t) \quad (4)$$

Therefore, it is seen that the difference of e_1 and e_2 can be controlled to regulate the AC current and power transfer, Furthermore the transfer function of the AC current model can be represented as

$$G_p(s) = \frac{1}{L_{eq}s + R_{eq}} \quad (5)$$

2.3 The analysis of optimal reactive power distributed in two power ends

The total equivalent interconnection inductor will consume certain amount of reactive power, which has to be compensated by both power ends of IMDCC, for example, if the total reactive power consumed by L_{eq} is 10MVar and half of these reactive power has been compensated by MMC1, then the rest of 50% reactive power has to be compensated by MMC2 (in two ends application like Figure 1(a)). However, the maximum power rating or installed power of each MMC is constant, the increasing compensated reactive power of one end means that its output active power will be decreased. Furthermore, the active power transferring capability of IMDCC is limited by the end which compensates larger reactive power and transfers less active power. Therefore, different reactive power distribution ratio between two ends has a great effect on the utilization of IMDCC, especially when the AC voltage is medium frequency and its reactive power will become quite significant.

Assuming that installed powers of both ends in IMDCC are identical, and the maximum power (or installed power) can be expressed as

$$S_{max} = \sqrt{P_j^2 + Q_j^2} \quad (6)$$

where S_{max}, P_j and Q_j are the installed power, active power and reactive power for both ends, respectively. It should be noted that S_{max} is a constant as determined by power rating of selected components, which is not influenced by the actual operation conditions.
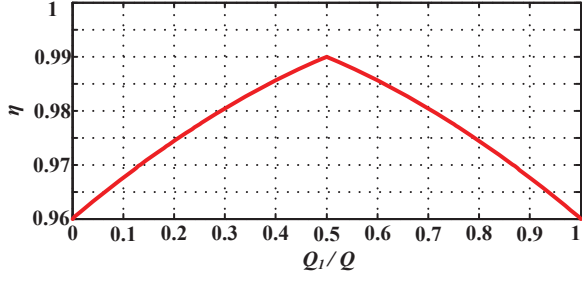
Figure 3: Relationships between utilization factor η and the ratio of reactive power distributed in MMC1.

Considering law of conservation of energy, active power flowing in both stations should be equivalent and then the actual maximum transmission active power can be written as

$$P_{max}{}^2 = \min\{P_1^2, P_2^2\} \quad (7)$$

Then the maximum reactive power can be given by

$$Q_{max} = Q_1 + Q_2 \quad (8)$$

Combining (6)-(10), that is

$$P_{max}{}^2 = \begin{cases} S_{max}{}^2 - Q_{max}{}^2\left(1 - \dfrac{Q_1}{Q_{max}}\right)^2, & \dfrac{Q_1}{Q_{max}} \in [0, 0.5) \\[4mm] S_{max}{}^2 - Q_{max}{}^2\left(\dfrac{Q_1}{Q_{max}}\right)^2, & \dfrac{Q_1}{Q_{max}} \in [0.5, 1] \end{cases} \quad (9)$$

In addition, a utilization factor η is defined as the ratio of actual maximum transferred active power divided by the maximum power:

$$\eta = \frac{P_{max}}{S_{max}} \quad (10)$$

Therefore, the utilization factor in relation with the different reactive power distribution is shown in Figure 3. It is concluded that the maximum utilization could be achieved when reactive power is distributed equally between both power ends of IMDCC.

2.4 Influence of distributed reactive power on the ripple of capacitor voltages

According to [11], power change of each arm is closely related to the operating status of convertor. Hence, the energy fluctuation ΔW_1 in one arm of MMC$_1$ can be described as

$$\begin{cases} \Delta W_1 = \dfrac{\lambda_1 S_{max}}{\omega}\left\{1 - \left[(m_1 \cos\varphi_1)/2\right]^2\right\}^{3/2} \\[4mm] \lambda_1 = \dfrac{U_{dc1}}{\sqrt{6}U_{N1}} \end{cases} \quad (11)$$

where U_{N1} is the RMS value of AC voltage in MMC$_1$, m_1 is its modulation ratio, and φ_1 is the shifted phase angle between AC voltage and AC current of MMC$_1$. Similarly, the energy fluctuation ΔW_2 in one arm of MMC$_2$ also can be described. Therefore, the total fluctuation ΔW of IMDCC can be obtained by the summation of ΔW_1 and ΔW_2:

$$\Delta W = \Delta W_1 + \Delta W_2 \quad (12)$$

Hence, a picture about the fluctuation in arms of IMDCC has been obtained in Figure 4. It can be concluded that the total fluctuation energy is the smallest when the reactive power is
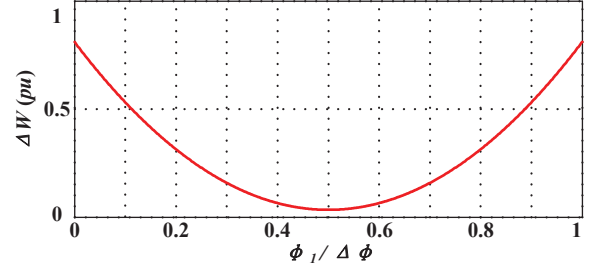
Figure 4: Relationships between the per unit value of energy fluctuation in the whole IMDCC system ΔW(pu) and the ratio of reactive power distributed.

distributed equally between two power ends. Therefore, the whole capacitor voltage ripple of IMDCC reaches the lowest value when the reactive power distributed evenly between both MMC ends. This feature may be beneficial to alleviate capacitor voltage ripples and reduce capacitance.

3 Control Strategies

In order to achieve the reactive power is distributed evenly between both ends as the above analysis, this section describes the control strategies, consisting of power flow management and capacitor voltage balancing regulation: the power flow control is intended for regulation of the transferred active/reactive power between MMC$_1$ and MMC$_2$, in order to achieve the optimal reactive power distribution, while capacitor voltage balancing control aims to eliminate the power unbalance which may occur among the capacitors of different SMs.

3.1 Control for optimal reactive power distribution

The reactive power Q_1 and Q_2 can be expressed by the RMS value of transformer currents I_{acj} and the RMS value of its terminal voltages U_{acj}, this is

$$\begin{cases} Q_1 = U_{ac1}I_{ac1}\sin\varphi_1 \\ Q_2 = U_{ac2}I_{ac2}\sin\varphi_2 \end{cases} \quad (13)$$

According to the relationship between currents and voltages of transformer

$$\frac{I_{ac1}}{I_{ac2}} = \frac{1}{n} \quad (14)$$

$$\frac{U_{ac1}}{U_{ac2}} = n \quad (15)$$

Then multiply (16) with (17), that is

$$I_{ac1}U_{ac1} = I_{ac2}U_{ac2} \quad (16)$$

if the IMDCC system operates in the optimal reactive power distribution mode, the relationship between Q_1 and Q_2 can be expressed as

$$Q_1 = U_{ac1}I_{ac1}\sin\varphi_1 = Q_2 = U_{ac2}I_{ac2}\sin\varphi_2 \quad (17)$$

namely,

$$\sin\varphi_1 = \sin\varphi_2 \quad (18)$$

Then it is concluded that the reactive power of IMDCC system can be distributed equally when the shifted phase angle φ_1 of MMC$_1$ is equal to the shifted phase angle φ_2 of
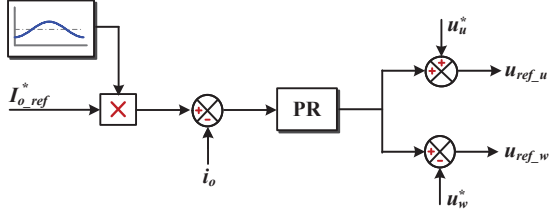
Figure 5: Power flow control by transient ac current

(a)

(b)
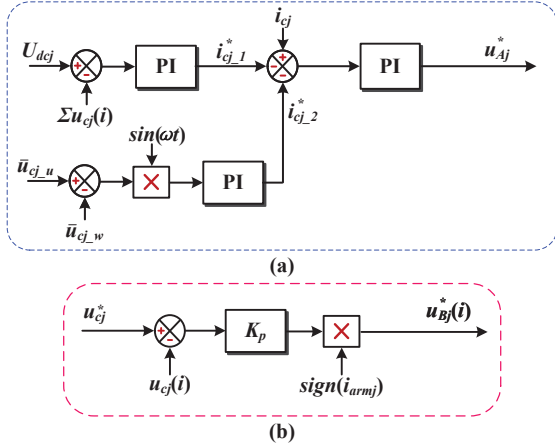
Figure 6: Capacitor voltage balancing control diagrams. (a) Phase balancing and arm balancing control; (b) SM balancing control

MMC$_2$, achieving the optimal reactive power distribution of IMDCC.

Furthermore, if in a single-phase IMDCC system, a proportional resonant (PR) control is needed to precisely track the AC current reference as to regulate the power flow directly. The control diagram is pictured in Figure 5 and the transfer function is

$$G(s) = K_p + \frac{2K_r \omega_c s}{s^2 + 2\omega_c s + \omega_0^2} \tag{19}$$

where K_p, K_r are respectively the control gains of the proportional and resonant controller, and ω_0 is the resonant frequency, ω_c is bandwidth of resonant controller. Furthermore, if the IMDCC system is a three-phase system, the power flow can be controlled indirectly by controlling the currents in traditional rotating d-q frame. However, it should be noted that since AC voltage commands for both MMC ends are generated by the same controller, only the AC currents need to be acquired form a current feedback control, without the need of a phase-locked loop (PLL) and ac voltage sensors.

3.2 Capacitor voltage balancing control

Like the traditional MMC, IMDCC comprises many floating dc capacitors and these capacitor voltages may deviate from the desired value because of the disturbance such as parasitic resistances and harmonics etc., which is also the common issue to be solved before operation. Hence, the traditional balancing control of MMC is also valid in IMDCC[12].

Table 1: Simulation Parameters

QUANTITY	VALUE
Number of SMs per arm	$N=3$
Number of phases per converter	Phase=1
Fundamental frequency	$f_o=100$Hz
Primary side DC voltage level	$V_{dc1}=300$V
Secondary side DC voltage level	$V_{dc2}=300$V
Rated SM capacitor voltage	$U_c=100$V
SM capacitance	$C=1860$μF
Buffer inductors	$L=2.5$mH
Carrier frequency	$f_c=3$kHz
Maximum modulation	$m_{max}=0.8$
Leakage inductance	$L_\sigma=6$mH
Peak-to-peak ac current	$i_{ac\_pp}=40$A

1) Phase and arm balancing control

The phase balancing control ensures that the energy stored in this phase in maintained balanced by controlling the total capacitor voltage Σu_{cj} and circulating current i_{cj}, which is given by

$$\sum u_{cj}(i) = \sum_{i=1}^{N}\left(u_{cj\_u}(i) + u_{cj\_w}(i)\right) \tag{20}$$

where the phase balancing controller compares the summation of capacitor voltages in one phase Σu_{cj} to the dc bus voltage U_{dcj}, generating the circulating current reference command $i^*_{cj\_1}$ via a PI controller. Similarly, the aim of arm balancing control compares the averaging value of upper arm to the averaging value of lower arm to ensure the energy stored in both arm balanced, which generates the circulating current $i^*_{cj\_2}$ via a second PI controller, then the controller forces the circulating current i_{cj} to follow its command $i^*_{cj\_1} + i^*_{cj\_2}$. The phase balancing and arm balancing control structure are depicted in Figure 6(a).

2) SM balancing control

As shown in Figure 6(b), the SM balancing control compares each capacitor voltage to the command u^*_{cj}, producing the adjusting value u^*_{Bj}. It is noted that the polarity changes with the direction of arm current i_{armj}.

$$u^*_{Bj}(i) = K_p\left(u^*_{cj} - u_{cj}(i)\right) \times sign(i_{armj}) \tag{21}$$

The generated reference will be eventually introduced into the corresponding PWM modulation.

4 Verifications of simulation and experiment

4.1 Simulation verification

A simulation model of the single-phase IMDCC has been built in Matlab/Simulink and the proposed optimal reactive power control strategy is verified. IMDCC consists of two convertors with one phase, and each phase has six SMs and two large buffer inductors which are evenly distributed between the upper and lower arms. The power flow direction is assumed to be from the U_{dc1} to U_{dc2} through a transformer
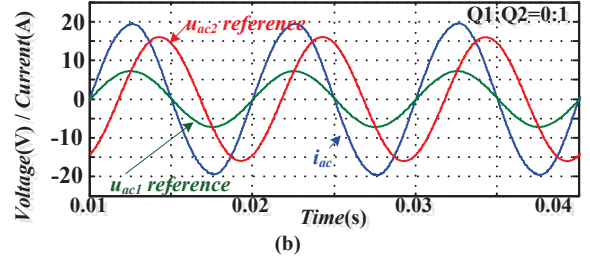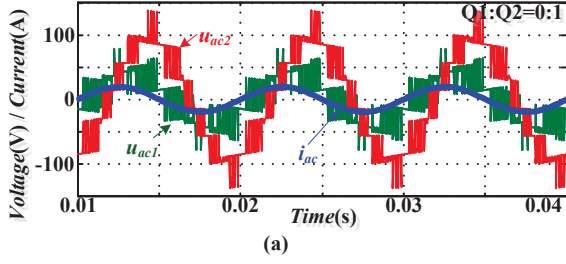
Figure 7: Simulation results when Q_1:Q_2=0:1. (a) AC voltages and current; (b) AC voltage references and AC current.
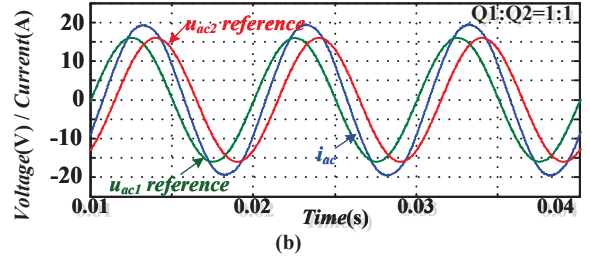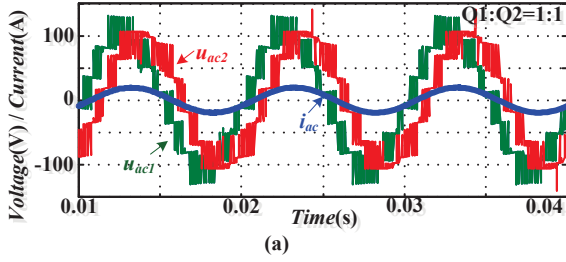
Figure 8: Simulation results when Q_1:Q_2=1:1. (a) AC voltages and current; (b) AC voltage references and AC current.
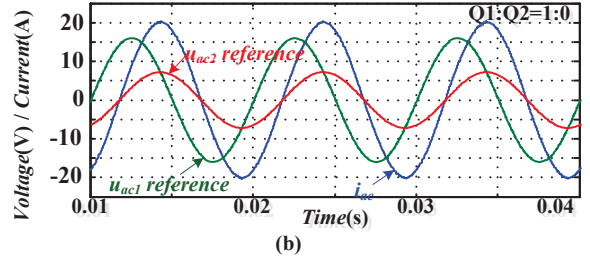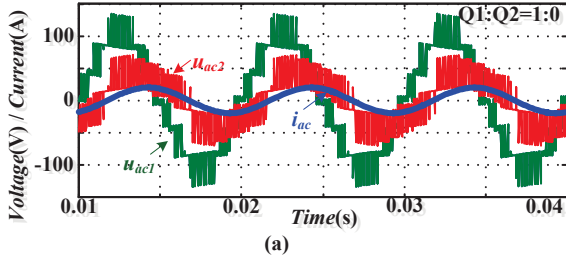
Figure 9: Simulation results when Q_1:Q_2=1:0. (a) AC voltages and current; (b) AC voltage references and AC current.

with ratio of n=1:1, where the maximum modulation ratio of AC voltage is set up as 0.8 so as to be reserved for controlling adjustment, and the peak-to-peak value of AC current is set as 40A. Other specifications and main parameters of the IMDCC system are shown in Table 1.

Figures 7~9 show the reference signals and simulation waveforms of u_{ac1}, u_{ac2} and i_{ac} under three different reactive power distribution ratios: Q_1:Q_2=0:1, Q_1:Q_2=1:1 and Q_1:Q_2=1:0, respectively. In Figure 7, MMC$_1$ is working in the unite power factor, as the corresponding ac voltage u_{ac1} is in phase with ac current i_{ac}. In this situation, the modulation of u_{ac1} has to be less than 0.5 since larger reactive power is compensated by MMC$_2$ and its transferred active power has to be less correspondingly. At the same time, the simulation waveforms in this condition are given in Figure 7(a), where the ac current is sinusoidal and its peak-to-peak value reaches 40A steadily.

Then, the reference signals and simulation waveforms of condition Q_1:Q_2=1:1, which the reactive power is distributed equally in both ends, are shown in Figure 8. In this situation, AC current is a sinusoidal wave, while both the voltage references u_{ac1} and u_{ac2} can also reach the maximum value at the same time. Therefore, it is reasonable that more active power can be transferred when reactive power is distributed equally in both ends of IMDCC.
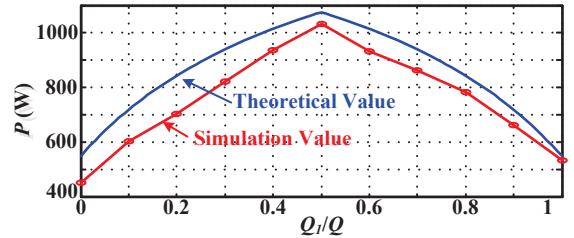
Figure 10: Simulation results of transferred active power in different ratio of reactive power distributed in both power ends of IMDCC.

Furthermore, the situation of Q_1:Q_2=1:0 is similar to the first condition in Q_1:Q_2=0:1, the simulation results have been described in Figure 9, where MMC$_2$ is working in the unite power factor and the transferred active power decreased as the result of larger active power is compensated by MMC$_1$.

Finally, Figure 10 shows the simulation results of transferred active power in different ratio of reactive power distribution, from the condition that the reactive power is compensated fully by MMC2 to condition that all reactive power is compensated by MMC1. It can be seen that the transferred power reaches the highest point when reactive power is distributed equally, which shows the validity of theoretical analysis and its control strategies.
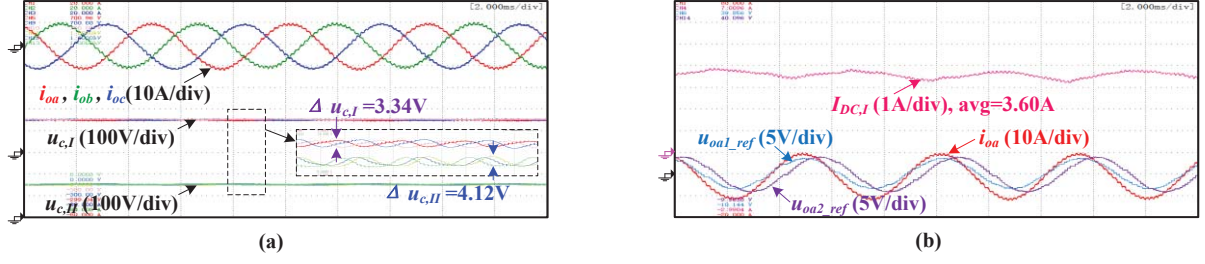
Figure 11: Experimental waveforms when Q_1:Q_2=0:1. (a) AC currents and capacitor voltages in both MMCs; (b) DC current and the comparison between the AC voltage references and the corresponding AC current.
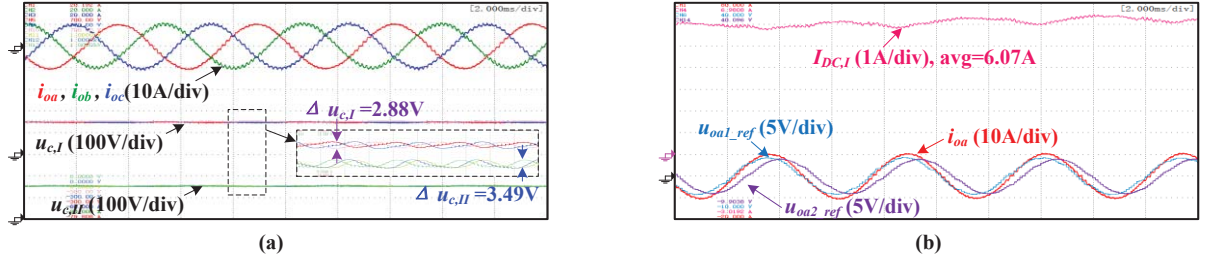
Figure 12: Experimental waveforms when Q_1:Q_2=1:1. (a) AC currents and capacitor voltages in both MMCs; (b) DC current and the comparison between the AC voltage references and the corresponding AC current.
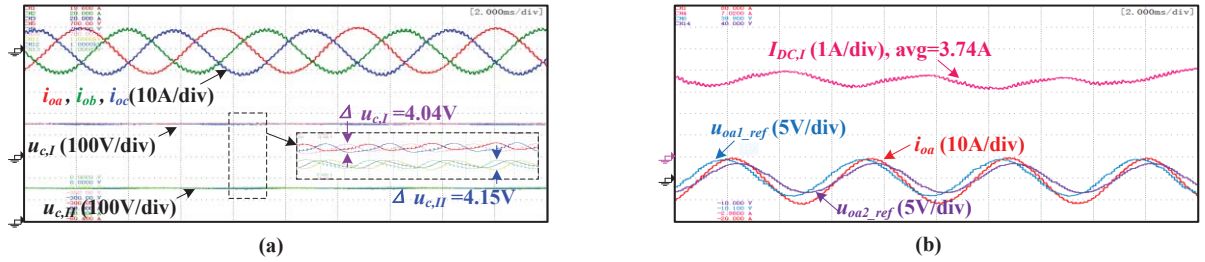
Figure 13: Experimental waveforms when Q_1:Q_2=0:1. (a) AC currents and capacitor voltages in both MMCs; (b) DC current and the comparison between the AC voltage references and the corresponding AC current.

4.2 Experimental verification

In order to further verify the theory of the optimal reactive power distribution control, a three-phase IMDCC experimental platform has been built, where the amplitude AC current is set as 10A constantly to make sure the same reactive consuming in the AC side. Specifically, since the reactive power consuming of AC-side inductance is proportional to the frequency, the AC-side fundamental frequency is set as 200Hz to intensively produce a higher reactive power than 50Hz/60Hz. Moreover, the fundamental frequency is set as a medium frequency to reduce the volume and weight of IMDCC system. The rest of experimental parameters are as follows: the DC bus voltage is $U_{dc1} = U_{dc1}$ =300V; the number of SM per arm is N=2; capacitance of each SM is C_{SM}=1000μF; arm inductance is L_{arm}=4mH; the leakage inductor is L_σ=1mH in AC side; maximum modulation is m=0.8; and the carrier frequency f_c=3kHz.

Firstly, experimental waveforms when the primary side MMC$_1$ is operated under unite power factor and the whole reactive power is compensated by the secondary station MMC$_2$ are shown in Figure 11. Although one side of IMDCC
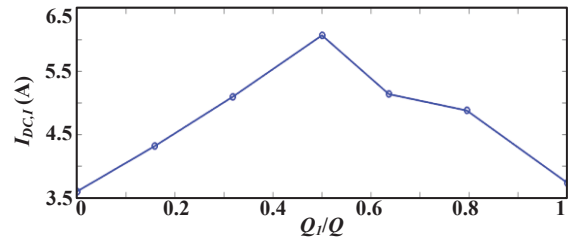
Figure 14: Experimental waveforms for the average value of DC currents in different ratio of reactive power distributed in four same tests.

is working in the condition that the corresponding AC voltage u_{ac1} is in phase with AC current i_{ac}, it only produces the average value of 3.6A in DC side, thus it only transferred 1.08kW active power from MMC$_1$ to MMC$_2$. It should be noted that there is an inevitable fluctuation in DC current since there are only 2 SMs per arm in this experiment. Moreover, it can be observed that the capacitor voltage fluctuations are with a peak-to-peak value of 3.34V for MMC$_1$, and 4.12V for MMC$_2$, respectively.

As shown in Figure 12, the reactive power is evenly distributed between both stations of IMDCC, where neither

AC voltage is not in phase with AC current, but the average value of 6.07A in DC side current and 1.82kW active power has been transferred from MMC_1 to MMC_2, thus the utilization η has been improved about 68% than the situation in Figure 11. Furthermore, the capacitor voltage fluctuations with a peak-to-peak value of 2.88V (MMC_1) and 3.49V (MMC_2) respectively, which has been alleviated about 14% than that in Figure 11. Therefore, the transferred active power can be improved and the voltage fluctuations in SMs can be decreased when the reactive power is distributed evenly between both stations of IMDCC.

Further experiment is carried out to test the transferred active power and capacitor voltage ripples when MMC_2 is worked in unite power factor (see Figure 13). There is only 3.74A (average value) in DC current but capacitor voltage ripples has been increased to 4.04V for MMC_1 and 4.15V for MMC_2, respectively. It is concluded again that the optimal reactive power distribution control can improve the transferred active power and reduce voltage fluctuations in SMs.

Finally, in order to test the transferred active power in different reactive power distribution ratio, the experimental waveforms under seven different reactive power distribution ratios are shown in Figure 14. Therefore, the maximum transferred active power can be achieved when the reactive power is distributed evenly between both stations.

5 Conclusion

In this paper, an optimal reactive power distribution control has been presented in the isolated modular DC/DC converter (IMDCC) system based on theoretical analysis, simulated discussions and experimental verifications. The system configuration ties two dc grids by using two modular multilevel converters (MMCs) via a galvanic isolation transformer, where the transformer and arm inductances cause the reactive power consuming and will affect the maximum transferring active power capability. The theoretical discussions conclude that the ratio of reactive power being equally distributed in both MMCs can get maximum active power transferring capability for the whole IMDCC system, which is also beneficial for alleviating the energy fluctuation of capacitors. Finally, the control methods are described along with simulated and experimental results that verify the proposed control method.

It should be noted finally that this study has only analysed and examined on the sinusoidal AC voltage, further study based on square wave or trapezoidal wave AC voltage is needed. Moreover, the fluctuant DC current in experiments has a negative impact on the measurement of average value, but this problem could be solved by more SMs per arm in the future.

Acknowledgements

References

[1] D. Westermann, D. Van Hertem; A. Küster, R. Atmuri, B. Klöckl, T. Rauhala, "Voltage source converter (VSC) HVDC for bulk power transmission - technology and planning method," in *AC and DC Power Transmission, ACDC. 9th IET International Conference on*, pp.1-6, 19-21 Oct. 2010.

[2] D. Jovcic, B. T. Ooi, "Developing DC Transmission Networks Using DC Transformers," *IEEE Transactions on Power Delivery*, vol. 25, no. 4, pp. 2535-2543, Sept. 2010.

[3] S. Kenzelmann, D. Dujic, F. Canales, Y. R. De Novaes, A. Rufer, "Modular DC/DC Converter: Comparison of Modulation Methods," *EPE/PEMC*, Sept. 2012.

[4] C. D. Barker, C. C. Davidson, D. R. Trainer, R. S. Whitehouse, "Requirements of DC-DC Converters to facilitate large DC Grids," *Proceeding of CIGRE Symposium*, Kansas: CIGRE, 2012: B4-204.

[5] M. Hajian, et al., "30kW, 200V/900V, Thyristor LCL DC/DC Converter Laboratory Prototype Design and Testing," *IEEE Transactions on Power Electronics*, vol. 3, no. 29, pp.1094-1102, 2014.

[6] J. A Ferreira, "The Multilevel Modular DC Converter," *IEEE Transactions on Power Electronics*, vol. 28, no. 10, pp. 4460-4465, Mar. 2013.

[7] A. Schon, and M. Bakran, "A New HVDC-DC Converter with Inherent Fault Clearing Capability," *EPE 15th European Conference on*, pp.1-10, Sept. 2013.

[8] W. Lin, "DC-DC Autotransformer with Bidirectional DC Fault Isolating Capability," *IEEE Transactions on Power Electronics*, vol. 31, no. 8, pp. 5400-5410, Mar. 2016.

[9] S. P. Engel, M. Stieneker, N. Soltau, S. Rabiee, H. Stagge, R. W. De Doncker, "Comparison of the Modular Multilevel DC Converter and the Dual-Active Bridge Converter for Power Conversion in HVDC and MVDC Grids," *IEEE Transactions on Power Electronics*, vol. 30, no. 1, pp. 124-137, Jan. 2015.

[10] S. Kenzelmann, A. Rufer, D. Dujic, F. Canales, Y.R. De Novaes, "Isolated DC/DC Structure Based on Modular Multilevel Converter," *IEEE Transactions on Power Electronics*, vol. 30, no. 1, pp. 89-98, Jan. 2015.

[11] W. Shanshan, Z. Xiaoxin, T. Guangfu, H. Zhiyuan, T. Letian, L. Jun "Selection and Calculation for Sub-module Capacitance in Modular Multi-level Converter HVDC Power Transmission System," *Power System Technology*, vol. 35, no. 1, pp. 26-32, 2011.

[12] M. Hagiwara, H. Akagi, "Control and experimental of pulsewidth modulated modular multilevel converters," *IEEE Transactions on Power Electronics*, vol. 24, no. 7, pp. 1737-1746, Jul. 2009.